ACS APPLIED MATERIALS & INTERFACES

www.acsami.org

Research Article

Triple Emulsion-Based Rapid Microfluidic Production of Core−Shell Hydrogel Microspheres for Programmable Biomolecular Conjugation

Eric Y. Liu, Yoon Choi, Hyunmin Yi,* and Chang-Hyung Choi*

Cite This: *ACS Appl. Mater. Interfaces* 2021, 13, 11579−11587

Read Online

ACCESS | Metrics & More | Article Recommendations | Supporting Information

ABSTRACT: We report a simple and rapid microfluidic approach to produce core−shell hydrogel microspheres in a single step. We exploit triple emulsion drops with sacrificial oil layers that separate two prepolymer phases, forming poly(ethylene glycol)-based core−shell microspheres via photopolymerization followed by spontaneous removal of the oil layer. Our technique enables the production of monodisperse core−shell microspheres with varying dimensions of each compartment by independently and precisely controlled flow rates. This leads to stable and uniform incorporation of functional moieties in the core compartment with negligible cross-contamination into the shell layer. Selective conjugation of biomolecules is enabled through a rapid bioorthogonal reaction with functional groups in the core compartment with minimal non-specific adsorption. Finally, in-depth protein conjugation kinetics studies using microspheres with varying shell porosities highlight the capability to provide tunable size-selective diffusion barriers by simple tuning of prepolymer compositions for the shell layer. Combined, these results illustrate a significant step forward for programmable high-throughput fabrication of multifunctional hydrogel microspheres, which possess substantial potential in a large array of biomedical and biochemical applications.

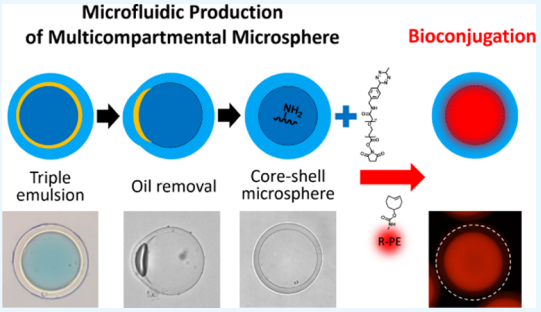

KEYWORDS: *core−shell microsphere, triple emulsion, microfluidics, biomolecular conjugation, hydrogel*

INTRODUCTION

Hydrogel microparticles offer significant utility in a broad range of applications including biosensing,[1,2] drug delivery,[3,4] catalyst support,[5] and directed self-assembly[6,7] due to their versatile properties from biocompatibility to simple tunability of the microenvironment in a three-dimensional polymeric network. Incorporation of biomolecules (e.g., micro-RNA, DNA, protein) or cells within the hydrogel network of microparticles enables the development of suspension arrays for multiplexed biosensing,[8,9] regenerative medicine,[10−12] or tissue engineering applications.[13,14] Particularly, multicompartmental particles have recently gained attention rising from the capability to impart discrete functionalities to each compartment within a single particle.[15−18]

Previously, several methods have been introduced to create monodisperse microspheres or microgels.[19−21] Particularly, precipitation polymerization or dispersion polymerization can enable production of multicompartmental polymeric spheres with submicron sizes.[22,23] While these approaches are versatile in creating core−shell microspheres with well-defined concentric geometry, it is difficult to control the particle size within a broad range from a few tens of micrometers to a few millimeters. In addition, there is a limited number of comonomers to choose from, preventing incorporation of a variety of functional moieties.[24]

Recent advances in microfabrication methods have led to the reliable production with controlled physical properties (e.g., size, shape, compartmentalization, and porosity),[25,26] which play a key role in determining their functionality. Specifically, spherical microparticles (i.e., microspheres) with multi-layered or core−shell architectures offer unique potential for controlling biomolecular diffusion limits toward a desired core compartment, potentially enabling size-selective bioconjugation or biosensing.

There currently exist two representative routes to create multicompartmental hydrogel microspheres: micromolding[27−29] and microfluidic technique[30−34] as a batch and continuous process, respectively. A promising micromolding technique involves sequential formation of primary and secondary compartments in micromolds via surface tension-induced droplet generation followed by photopolymerization for the production of Janus and core−shell microspheres with

Received: November 12, 2020
Accepted: February 18, 2021
Published: March 2, 2021

https://dx.doi.org/10.1021/acsami.0c20081
ACS Appl. Mater. Interfaces 2021, 13, 11579−11587

controllable size and shape.[27,35] Microfluidic techniques enable continuous manufacture of multicompartmental microspheres with tunable size and shape; approaches including emulsion template synthesis,[32,33] particle reinjection,[36] and centrifuge-based droplet formation[31,37] have been successfully enlisted.

However, there still exist unmet needs for simple and rapid production of multicompartmental microspheres with stable biomolecular conjugation and controlled size selectivity. While existing microfluidic techniques utilizing biphasic drops as templates can provide powerful means for mass production of Janus microspheres with varying compartment ratios,[32,33] it is difficult to create core−shell hydrogel microspheres that consist of very similar materials due to their miscibility. Alternatively, microfluidic methods based on particle re-injection allow production of chemically functional multi-compartmental microspheres,[36] yet they require multiple steps to load the primary compartment within prepolymer drops for the secondary one before polymerization, implying low throughput and inefficient processes. In addition, during the reinjection process, reactive chemicals within the prepolymer drops can penetrate within the hydrogel network, resulting in chemical cross-contamination and poorly defined functionalities. Thus, production of core−shell hydrogel microspheres in a rapid, high-throughput microfluidic fabrication method would represent a significant step forward in a number of biomedical and biochemical process applications.

Our approach to address these challenges is a microfluidic fabrication based on triple emulsion drop templates[38−42] integrated with post-biofunctionalization via selective biomolecular conjugation reactions. In this report, we present a novel one-step capillary microfluidic method to produce core−shell microspheres in a simple, rapid, and efficient manner. Specifically, we use triple emulsion drops with thin sacrificial oil layers that separate two prepolymer phases, resulting in poly(ethylene glycol) (PEG)-based core−shell microspheres via ultraviolet (UV) light-initiated free radical polymerization followed by spontaneous removal of the thin oil layer. First, results on size distribution of the microspheres show that our technique enables independent tuning of core−shell compositions and yields microspheres with high uniformity and tunable dimensions simply by controlling the flow rates. Small-molecule fluorescent labeling of the microspheres exhibits stable incorporation and uniform distribution of functional moieties in the core compartment without nonspecific adsorption or cross-contamination into the shell layer. We next show rapid biomolecular conjugation using model fluorescent proteins via a rapid bioorthogonal reaction with functional groups in the core compartment, again with minimal non-specific adsorption. In-depth protein conjugation kinetics studies with varying PEG shell contents show the capability to provide tunable size-selective diffusion barriers by simply changing the shell prepolymer compositions. Combined, these results support a significant step forward for programmable high-throughput fabrication of multifunctional hydrogel microspheres. We envision that the methods presented here can be readily expanded to overcome limitations in existing technologies for a range of application areas including rapid biosensing, medical diagnostics, and biological threat detection in suspension array formats requiring a minimal volume of complex biological samples.

RESULTS AND DISCUSSION

Rapid Capillary Microfluidic Fabrication of Functional Core−Shell Hydrogel Microspheres. We first demonstrate rapid and potent microfluidic production of core−shell hydrogel microspheres by utilizing triple emulsion drops with thin oil layers as sacrificial layers, as shown in the schematic diagram of Figure 1A. For this, we used a glass capillary microfluidic device consisting of three circular capillaries with varying orifice sizes all assembled into a square capillary. First, two circular capillaries for injection and collection are chemically treated to have hydrophobic surfaces with *n*-octadecyltrimethoxyl silane. This leads to stable fluid flow guided by wettability. The injection and the collection capillaries are then precisely aligned coaxially within the square capillary. In addition, a smaller tapered circular capillary is inserted into the injection capillary. Finally, the collection capillary is connected to a polyethylene microtubing where UV-initiated free radical polymerization occurs before the resulting microspheres are collected in a water container.

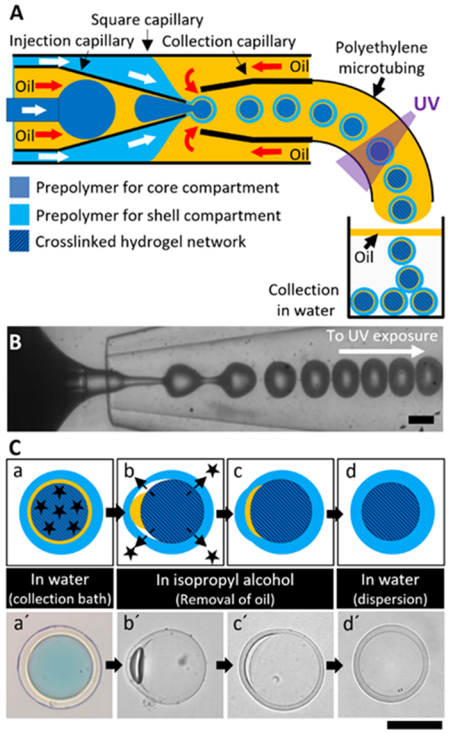

Figure 1. One-step capillary microfluidic production of core−shell PEG hydrogel microspheres by utilizing triple emulsion drops with a sacrificial oil layer. (A) Schematic diagram showing the glass capillary microfluidic device used to prepare triple emulsion drops. These drops are crosslinked via UV-induced free radical polymerization and collected in water to separate the outer oil phase from the polymerized microspheres. (B) Bright-field micrograph showing the formation of triple emulsion drops that flow through the collection capillary. (C) Schematic diagrams and the corresponding micrographs showing the sequence of core−shell microsphere formation; (a,a′) Blue dye in the innermost compartment shows the sacrificial oil layer between two compartments remains in water. Upon addition of IPA, (b,b′) the oil layer is initially dewetted from each compartment and (c,c′) thoroughly removed in half an hour, making core−shell microspheres (d,d′). Scale bar represents 100 μm.

To produce triple emulsion drops, an aqueous hydrogel prepolymer solution [10 vol % poly(ethylene glycol) diacrylate

https://dx.doi.org/10.1021/acsami.0c20081
ACS Appl. Mater. Interfaces 2021, 13, 11579−11587

(PEGDA) with 1 vol % photoinitiator (PI), Q_{IW}] is supplied through the smaller tapered capillary to form the innermost drop. An oil phase (*n*-hexadecane with 2 wt % Span 80, Q_{IO}) is supplied through the injection capillary to form a thin oil layer. These coaxial biphasic flows in the injection capillary result in a periodic stream of plug-like prepolymer drops in oil phase (i.e., water-in-oil) due to the strong affinity of the oil phase to the hydrophobically treated injection capillary. This flow pattern creates a lubrication oil layer between the innermost drop and the hydrophobic wall of the injection capillary, forming a thin oil layer within the emulsion drop. Next, additional prepolymer solution (10 vol % PEGDA with PI, Q_W) is supplied in a co-current fashion through the interstices between the injection capillary and the square capillary. The resulting triphasic fluid stream from the right-hand side is emulsified by an outer oil phase (mineral oil with 2 wt % Span 80, Q_O) at the exit of the injection capillary, forming monodisperse triple emulsion drops with a thin oil layer, as shown in Figure 1B (the interfacial tension values among the comprising fluids for the emulsion drop and viscosity of each fluid are listed in Table S1). This procedure creates a highly stable multiphasic fluid flow that enables continuous production of uniform triple emulsion droplets for over 2 h or longer (i.e., approximately 1,080,000 droplets/h), as illustrated in the video in Movie S1 (Supporting Information). These triple emulsion drops are then immediately exposed to UV illumination (estimated exposure time: 5 s) within 1 s to allow photopolymerization of the two hydrogel prepolymer phases, resulting in monodisperse core−shell hydrogel microspheres with the thin oil layer in between. This rapid process minimizes any undesired reagent transport between the two aqueous phases potentially rising from the surfactants while flowing through the microtubing.

As shown in the schematic diagram and the micrographs of (Figure 1C-a,a′), a water-soluble blue dye added into the core compartment remains separated from the shell compartment by the thin oil layer throughout polymerization and collection into water. This result clearly indicates that the two compartments are separated by the oil layer that completely prevents mass transport between them. Importantly, this result also suggests that we can impart chemical functionalities into the separate compartments in an independently controlled manner with negligible cross-contamination. Upon addition of isopropyl alcohol (IPA), the thin oil layer is partially dewetted from each compartment, and the blue dye encapsulated within the core compartment diffuses out through the shell compartment (Figure 1C-b,b′). The oil layer is gradually dissolved in IPA (Figure 1C-c,c′) and then completely removed (Figure 1C-d,d′), leaving hydrogel microspheres with segregated compartments upon dispersion into water. In short, our simple and rapid triple emulsion-based microfluidic approach yields core−shell hydrogel microspheres with core−shell geometry with negligible cross-contamination.

Production of Highly Uniform Core−Shell Microspheres with Controllable Compartment Ratios and Dimensions. As shown in Figure 2, our microfluidic approach enables production of highly uniform core−shell microspheres with controllable compartment ratios and dimensions. For this, we utilized triple emulsion drops with identical compositions in Figure 1 and varied the volume of each compartment by simply changing the flow rates of fluids. The as-prepared microspheres were examined via bright-field microscopy and the monodispersity was estimated by calculating the coefficient

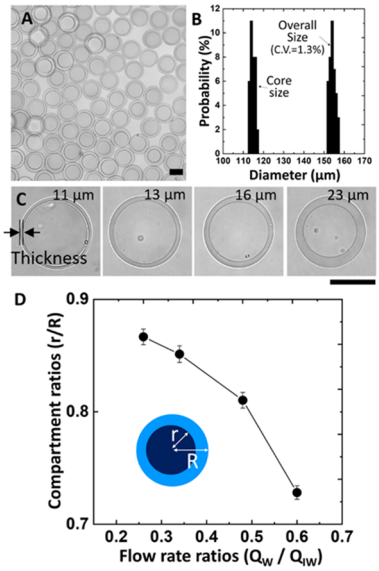

Figure 2. Tunability of core−shell microspheres. (A) Bright-field micrograph of core−shell microspheres with uniform size. (B) Size distribution of the overall and core sizes (CV = 1.3%). (C) Bright-field micrographs of microspheres with varying shell compartment thicknesses. Scale bars represent 100 μm. (D) Plot of compartment ratios (r/R) vs flow rate ratios (Q_W/Q_{IW}).

of variation (CV, %), defined as the ratio of the standard deviation to the mean size. The bright-field micrograph in Figure 2A shows the formation of uniform core−shell microspheres in a rapid manner; the detailed core−shell geometry of the resulting microspheres is clearly shown in the scanning electron microscopy (SEM) images of Figure S1. Figure 2B (and Figure S2) shows the narrow size distribution of the core compartment, overall microspheres, and shell thickness, clearly indicating their uniformity; the size distribution of each batch (i.e., total five batches, 1.3% CV for the entire population of 100 particles per batch) is consistent, demonstrating the reproducibility and robust nature of our method. Furthermore, the shell thickness of the microspheres is readily tuned by controlling the flow rates. For example, Figure 2C exhibits the varying shell thicknesses ranging from 11 to 23 μm by controlling the flow rates of the prepolymer solution (10 vol % PEGDA) for the shell compartment (1300−3000 μL/h, Q_W) and the core compartment (2000−3700 μL/h, Q_{IW}); the flow rates of other phases (Q_{IO} and Q_O) are fixed. Figure 2D demonstrates that our approach can be readily expanded to produce core−shell microspheres over a wide range of compartment size ratios (core/overall radius, r/R) by controlling the flow rate ratios (Q_W/Q_{IW}). Specifically, at a low flow rate ratio, we can produce the microspheres with a high compartment size ratio (0.87), while the compartment ratio is reduced to 0.7 with increasing flow rate ratio. The solid dots in Figure 2D show that compartment ratios can be readily tuned in a simple and reproducible manner, as indicated by the consistently small error bars obtained for all the conditions examined.

Compared to two-step microfluidic approaches based on particle reinjection,[5,36] the results in Figures 1 and 2 show that our method presents several distinct advantages. First, our approach provides a one-step production of core−shell hydrogel microspheres in a simple, robust, and rapid manner, unlike the particle reinjection-based approach that requires

https://dx.doi.org/10.1021/acsami.0c20081
ACS Appl. Mater. Interfaces 2021, 13, 11579−11587

redispersion of the as-prepared microspheres for the core compartment within prepolymer solution drops for the shell compartment prior to polymerization process (e.g., UV-initiated free radical polymerization); these characteristics should allow for sufficient production yield for applications to fine chemical industries such as pharmaceutics, cosmetics, and biomedicine. Second, our method enables production of multifunctional particles with independent chemistries in each compartment with negligible cross-contamination due to the thin oil layer (in triple emulsion drops) that plays a role in a diffusion barrier; otherwise the prepolymer for the shell compartment may diffuse into the core compartment through the pores in the polymer networks, causing undesirable chemical contamination and hence inconsistent functionalities. Third, our approach enables production of concentric (i.e., symmetric) core−shell microspheres with relatively uniform shell thickness, while the particle reinjection-based approach leads to a skewed core position (i.e., non-uniform shell thickness) due to the inherent limitation of the density difference between the solidified core compartment and the prepolymer drop for the shell compartment before UV exposure.[5] In short summary, results in Figure 2 demonstrate high fidelity and exquisite control over the microspheres afforded by simple microfluidic tuning in our method.

Flow Patterns for Stable Triple Emulsion Drops in the Capillary Device. Next, we examined the flow patterns as function of the flow rates of each fluid used for the triple emulsion drops. The phase diagram in Figure 3A (and Movies S1−S4) depicts typical patterns of the multiphase flow formed in the microfluidic device: (a) jetting, (b) non-uniform, (c) triple emulsion, and (d) separated flow. Here, the *y*-axis represents the flow rate of the 10 vol % PEGDA prepolymer solution for the shell compartment (Q_W), while the *x*-axis represents the sum of flow rates of the identical prepolymer solution for the core compartment (Q_{IW}) and the thin oil phase flow (*n*-hexadecane with surfactants, Q_{IO}), which are injected simultaneously through the injection capillary ($Q_I = Q_{IW} + Q_{IO}$). The outer oil phase (Q_O) is maintained at a fixed flow rate.

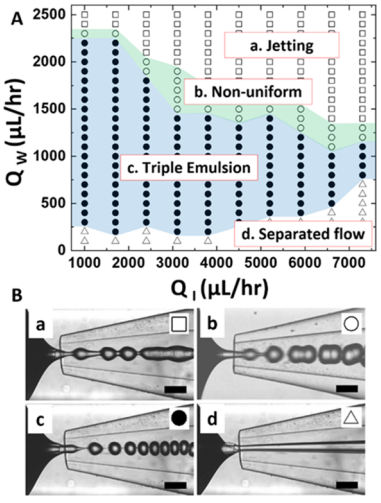

Figure 3. Flow patterns generated in the capillary microfluidic device. (A) Phase diagram showing flow behavior as a function of flow rate of the prepolymer solution for the shell compartment (Q_W, *y* axis) and sum of flow rates ($Q_I = Q_{IW} + Q_{IO}$, *x* axis) of the prepolymer solution for the core compartment (Q_{IW}) and the sacrificial oil phase flow (Q_I). (B) Bright-field micrographs showing (a) jetting, (b) non-uniform, (c) triple emulsion, and (d) separated flow, which are denoted as open square, open circle, solid circle, and open triangle, respectively. Scale bars represent 300 μm.

For high Q_W, jets (open squares, a) occur at any given Q_I. Due to relatively large flow rate ratio (Q_W/Q_I), the jets do not break up into droplets while strong shear force is applied (i.e., high Q_O). In contrast, for a slightly lower Q_W, the jets are emulsified in the dripping−jetting transition state, forming non-uniform emulsion drops with different numbers of cores (open circles, b). As Q_W is further reduced, the jets are consistently emulsified in the dripping mode, producing monodisperse triple emulsion drops with a single core (solid circles, c). With further reduction in Q_W, the flow rate of Q_W is not sufficient to fully surround Q_I, causing a displacement of the inner stream from the coaxial flow resulting in separated jet flow (open triangles, d). The possible regions for uniform triple emulsion become narrower with increasing Q_I; this implies that flow rate ratios play a key role in achieving successful triple emulsion formation with Q_I that is fully surrounded by Q_W while serving as a simple yet potent process parameter to control compartment size ratio. In short summary, the phase diagram shown in Figure 3 establishes a crucial relationship among relative flow rates while providing windows of readily controllable parameters for reliable manufacturing of triple emulsion drops.

Chemical Functionality of Chitosan−PEG Core−Shell Microspheres. Next, to investigate the post-fabrication biofunctionalization approach in a spatially discrete manner, we fabricated core−shell microspheres with the core compartment containing a potent aminopolysaccharide chitosan (CS) by simply adding soluble short-chain CS in the prepolymer solution. As shown in Figure 4A, a simple fluorescent labeling was employed to first examine the incorporation and chemical functionality of CS; the unshared electron pair of the primary amine group in each glucosamine unit of CS attacks the electron-deficient carbonyl carbon of the *N*-hydroxysuccinimidyl form of carboxyfluorescein (NHS-fluorescein) in an acyl substitution reaction yielding a stable amide bond.[29] For this, we fabricated microspheres with 10 vol % PEGDA and 0−0.8 wt % CS for the core and 10 vol % PEGDA for the shell compartment, respectively. The as-prepared microspheres were then exposed to a constant excess concentration of NHS-fluorescein (404 Da). The resulting fluorescence profile thus shows the presence and spatial distribution of CS's amine groups within the microspheres, as described in our previous works.[35,43]

First, the bright-field micrographs in Figure 4B show that the microspheres fabricated with our method display uniform sizes of both the core and shell compartments, consistent with the uniformity shown in Figure 2. Next, the corresponding epifluorescence micrographs in Figure 4B show minimal fluorescence without CS and increasingly bright and uniform fluorescence prepared with 0.2 and 0.8 wt % CS, indicating minimal nonspecific adsorption of NHS-fluorescein as well as the uniform distribution of the primary amines predominantly within the core compartment. Furthermore, minimal fluorescence in the shell compartments of CS−PEG microspheres, comparable to the ones prepared without CS, provides further evidence that the CS functional groups did not leak out into the shell compartments during particle fabrication. Finally, the total background-adjusted fluorescence intensity versus CS content plot in Figure 4C shows a linear increase in

https://dx.doi.org/10.1021/acsami.0c20081
ACS Appl. Mater. Interfaces 2021, 13, 11579−11587

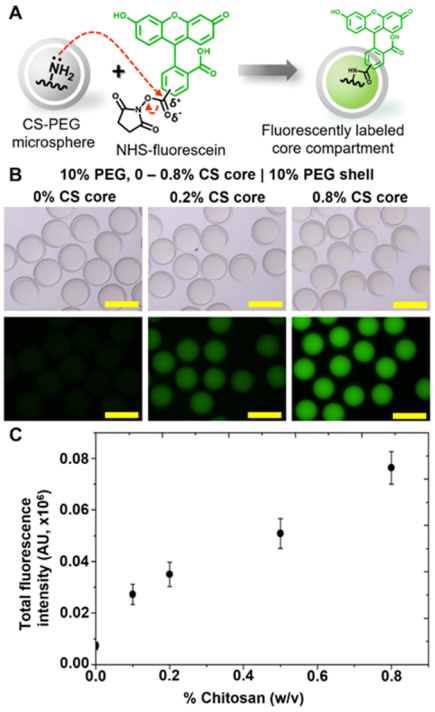

Figure 4. Fluorescent labeling with CS−PEG core−shell microspheres. (A) Schematic diagram of NHS-fluorescein labeling. (B) Bright-field (top row) and epifluorescence (bottom row) micrographs of the fluorescently labeled microspheres prepared with increasing CS content in the core compartment. Scale bars represent 200 μm. (C) Plot of total fluorescence intensity vs wt % CS in the core compartment.

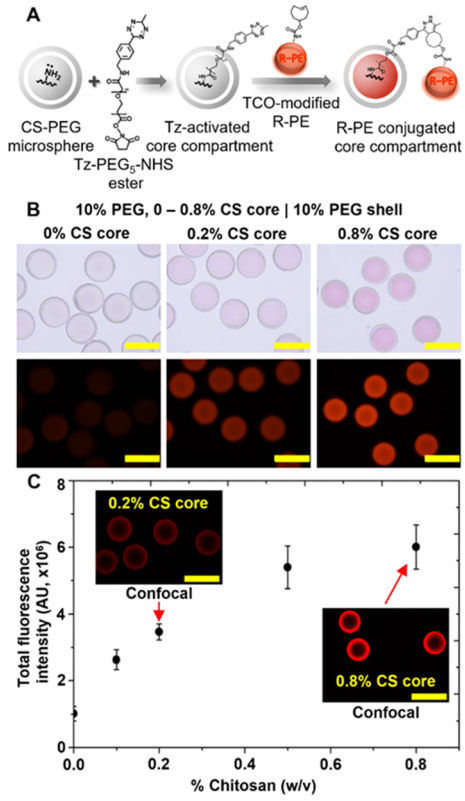

Figure 5. TCO-modified R-PE conjugation with CS−PEG core−PEG shell microspheres via Tz-TCO chemistry. (A) Schematic diagram of TCO-modified R-PE conjugation with CS-containing core compartment via Tz-TCO chemistry. (B) Bright-field (top row) and epifluorescence (bottom row) micrographs of TCO-modified R-PE conjugation with increasing CS content in the cores. (C) Plot of total fluorescence intensity vs CS (%, w/v) in the core compartment with corresponding confocal micrographs showing hindered diffusion into the center of the core compartment. Scale bars represent 200 μm.

fluorescence intensity with increasing CS content in the core prepolymer solution, indicating that we can readily control the capacity of functional groups within the core compartment. Combined, fluorescent labeling with small molecule dye NHS-fluorescein in Figure 4 indicates that our method allows for the controlled fabrication of functional microspheres with tunable and spatially discrete core functionality.

Selective Protein Conjugation with CS−PEG Core−Shell Microspheres. We next examined the conjugation of a large model protein R-phycoerythrin (R-PE, MW 240 kDa, hydrodynamic diameter $D_h \approx 11$ nm)[29,44] via rapid bioorthogonal tetrazine-*trans*-cyclooctene (Tz-TCO) chemistry[45] with microspheres prepared by 10 vol % PEGDA, 0−0.8 wt % CS core, and 10 vol % PEGDA shell prepolymer solutions. For this, as shown in the schematic of Figure 5A, we first converted the primary amines of CS in the core compartment to tetrazines (Tz) by reacting them with excess Tz-PEG5-NHS ester for 1 h. Upon washing away unreacted excess Tz, we then reacted these Tz-activated microspheres with 2 μM TCO-modified R-PEs for 2 h and examined their fluorescence, as described in our previous work.[35]

As shown in the bright-field micrographs in Figure 5B, microspheres with increasing CS content displayed increasingly red color exclusively in the core compartment upon R-PE conjugation with no color change in the shell compartment, suggesting that R-PE has penetrated the shells and reacted with the Tz in the cores. This observation is further evidenced in the corresponding epifluorescence micrographs of Figure 5B, in which microspheres with increasing CS core content show increasingly bright fluorescence in contrast to the minimal fluorescence of the shell compartment and the negative control (i.e., 0 wt % CS). Finally, the plot of total fluorescence intensity versus CS content in Figure 5C shows a non-linear increase in fluorescence with increasing CS core content, unlike the linear trend in Figure 4C. This difference is likely due to the hindered diffusion of R-PEs arising from the increase in CS content as described in our recent work.[35] In addition, the confocal micrographs of the CS−PEG microspheres show dim centers of the core compartment, indicating that the R-PE has not fully penetrated the core by 2 h of the reaction period.[29,35] Combined, these results successfully demonstrate the diffusion of large model proteins through the microspheres' shell compartments and subsequent diffusion and reaction within their core compartment with minimal nonspecific adsorption.

Protein Conjugation Kinetics within Core−Shell Microspheres with Varying PEG Contents of Shell Compartments. Finally, we examined the effect of PEG content in the shell compartment on the diffusion and reaction of two model fluorescent proteins of different sizes, green fluorescent protein (GFPuv) (27 kDa, $D_h \approx 5.5$ nm)[46] and R-PE (240 kDa, $D_h \approx 11$ nm), with the microspheres prepared with 10 vol % PEGDA, 0.5 wt % CS core, and 10−30 vol % PEGDA shell prepolymer solutions. For this, we used the same Tz-TCO chemistry with Tz-activated core compartments and TCO-modified GFPuv's and R-PEs to covalently couple the proteins with the cores, taking sample measurements at various

https://dx.doi.org/10.1021/acsami.0c20081
ACS Appl. Mater. Interfaces 2021, 13, 11579−11587

time points up to 8 h. The Tz-TCO reaction is very rapid ($k \approx 820\ M^{-1}\ s^{-1}$),[47] making the observed fluorescence dependent primarily on the diffusion of the proteins through the hydrogel networks.

First, as shown in the first row of the epifluorescence micrographs in Figure 6A, CS−PEG microspheres with 10% PEG shells displayed bright and uniform fluorescence within and among cores at 30 min, with a similar fluorescence at 1, 2, and 4 h, suggesting that the reaction has reached completion. This result indicates that GFPuv has diffused through the 10% PEG shells and reacted with the available Tz in the cores within 30 min. Meanwhile, there is minimal fluorescence in the shell compartment for all the conditions examined, again indicating minimal nonspecific adsorption and reliable fabrication of spatially discrete domains. A similar result is observed for the 20% PEG shell condition, with a slightly brighter core fluorescence compared to the cores in the 10% PEG shell condition at all time points examined.

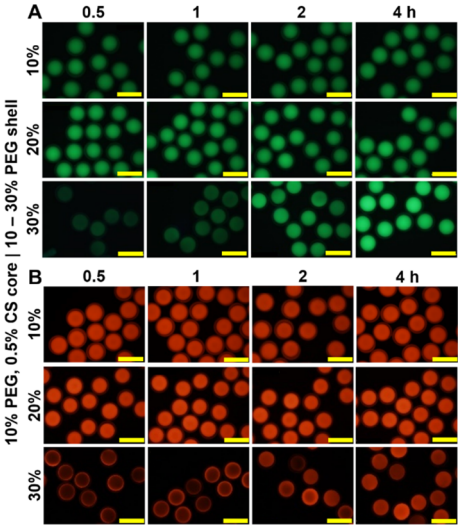

Figure 6. Epifluorescence micrographs of (A) GFPuv and (B) R-PE conjugation with CS−PEG core−shell microspheres prepared with 10% PEGDA, 0.5% CS core, and 10−30% PEGDA in the shell compartment. Increasing PEG content in the shell compartment results in delayed increase in fluorescence, indicating hindered protein diffusion. Scale bars represent 200 μm.

We attribute this to a small amount of PEGDA from the 20% shell region diffusing inward through the oil layer into the core compartment during polymerization driven by concentration gradient, thus leading to slightly more PEG in the core compartments. An increase in PEG may result in better incorporation of CS via inefficient Michael addition reaction,[48] thereby leading to more primary amines and brighter fluorescence.

Next, the third row of micrographs in Figure 6A shows a much dimmer fluorescence for the 30% PEG shell condition microspheres at 30 min, followed by gradually increasing fluorescence with time, plateauing by 4 h. We attribute this to the smaller mesh size of the 30% PEG shells significantly retarding the diffusion of GFPuv to the cores. Meanwhile, CS−PEG microspheres prepared with 10% PEG, 0.5 wt % CS core, and 40 vol % PEGDA shell prepolymer solution showed minimal fluorescence for all time points (data not shown), indicating that the 40% PEG shells largely exclude the GFPuv's from diffusing into the cores to react with the available Tz on CS.

A similar trend is observed for R-PE conjugation in the epifluorescence micrographs of Figure 6B. Again, the 10 and 20% shell conditions show relatively uniform and similar fluorescence in the cores at all time points, with the cores of the 20% PEG shell condition consistently brighter than those of the 10% one. However, the centers of the individual cores are consistently dimmer than the outer core compartments, suggesting that the R-PE has not diffused completely within the centers of the cores. This contrasts with the GFPuv results and is likely due to R-PE having roughly twice the hydrodynamic diameter (i.e., smaller diffusion coefficient) than GFPuv.

Intriguingly, capillary microfluidics-based microspheres without the shell layer (as described in our previous work[35]) fabricated using the same 10 vol % PEGDA, 0.5 wt % CS prepolymer composition as the microsphere's cores exhibited full penetration of TCO-R-PE upon 4 h of conjugation via Tz-TCO chemistry at lower TCO-R-PE concentrations. Taken together, this suggests that the presence of the PEG shell presents a significant barrier to the diffusion (and thus subsequent reaction) of R-PE even at the same PEG concentration in the core. This is likely because the core−shell microsphere fabrication may lead to higher PEG and CS contents in the core compartments compared with single microsphere fabrication, as the PEGDA in the cores may diffuse out into the oil phase at a slower rate. Finally, the third row of Figure 6B shows non-uniform fluorescence both within and among cores of the 30 vol % PEG shell condition, slowly increasing with time. This is likely due to the decreased mesh size of the 30 vol % PEG shells significantly hindering the diffusion of R-PE. The non-uniformity could arise if there is significant heterogeneity in pore size distribution of the shells, causing some shells to allow more rapid diffusion of R-PE than others. Combined, the results in Figure 6 show that the shell compartments of CS−PEG microspheres can provide attractive size-selective barriers to selectively hinder or completely exclude the diffusion of proteins based on size simply by changing the prepolymer composition of the shells.

CONCLUSIONS

In this work, we presented a straightforward, one-step capillary microfluidic method to fabricate core−shell hydrogel microspheres based on triple emulsion drops. This technique allows for independently tunable core and shell prepolymer compositions and yields microspheres with highly uniform and tunable shell dimensions by precisely controlling the flow rates. We also presented a phase diagram detailing the operating flow rate ranges for consistent triple emulsion drop formation, representing a potent approach for manipulating multiphasic fluids for fabricating functional materials by utilizing complex emulsion templates. Small-molecule fluorescent labeling studies showed stable incorporation and uniform distribution of CS's primary amine functional moieties in the core compartment with minimal functional moiety diffusion out to the shell during the fabrication process. Epifluorescence micrographs of the TCO-modified R-PE conjugation with the microparticles via Tz-TCO chemistry illustrated rapid protein conjugation in the core compartments with minimal nonspecific adsorption. Finally, kinetics studies with TCO-modified GFPuv and R-PE with CS−PEG microspheres prepared with varying PEG shell contents demonstrate

https://dx.doi.org/10.1021/acsami.0c20081
ACS Appl. Mater. Interfaces 2021, 13, 11579−11587

the ability to provide tunable size-selective diffusion barriers by simply changing the shell prepolymer compositions. While this work demonstrated the use of the shell compartments as a simple barrier based on size, one can envision functionalizing the shell compartment as well as two distinct functional modules in the core and the shell to impart multi-functional selectivity, allowing for the isolation of specific molecules of interest in complex biological mixtures. Combined, these results demonstrate the high potential of our rapid microfluidic approach for manufacture of a variety of multifunctional microspheres toward a variety of applications in cosmetics, biosensors, catalysis, and display.

MATERIALS AND METHODS

Materials. Tween 20, borate buffered saline (20× concentrate, 50 mM borate, pH 8.5), Luria−Bertani media, ampicillin, isopropyl β-D-1-thiogalactopyranoside, and Bradford assay kits were purchased from Thermo Fisher Scientific (Waltham, MA). BugBuster reagent and centrifugal filter units (Amicon Ultra 0.5 mL) were purchased from EMD Millipore (Billerica, MA). Hexadecane (99%), mineral oil, PEGDA (M_n 700 Da), CS oligosaccharide lactate (average M_n 5 kDa, >90% deacetylation), 2-hydroxy-2-methylpropiophenone, poly(vinyl alcohol) (87−89% hydrolyzed), *n*-octadecyltrimethoxyl silane, sorbitane monooleate (Span 80), PEG-*block*-poly(propylene glycol)-*block*-PEG (F108), IPA (99.5%), ethanol (99.8%), erioglaucine disodium salt, saline sodium citrate buffer (SSC) (20× concentrate, pH 7.0), and phosphate buffered saline (10 mM phosphate, 2.7 mM potassium chloride, 137 mM sodium chloride) pH 7.4 were purchased from Sigma-Aldrich (St. Louis, MO). 5- (and 6-)carboxyfluorescein succinimidyl ester (NHS-fluorescein) was purchased from Pierce Biotechnology (Rockford, IL). Dimethyl sulfoxide was purchased from Acros Organics (Geel, Belgium). R-PE was purchased from AnaSpec Incorporated (Fremont, CA). TCO-PEG4-NHS ester and Tz-PEG5-NHS ester were purchased from Click Chemistry Tools (Scottsdale, AZ). Imidazole was purchased from Amresco (Solon, OH). ABIL EM 90 was purchased from Evonik Industries (Germany). 2-[Methoxy(polyethyleneoxy)propyl] trimethoxy silane was purchased from Gelest (Morrisville, PA). *Escherichia coli* BL 21 harboring the plasmid *ptrcHisB::gfpuv* were generously provided by Dr. Chen-Yu Tsao and Dr. William E. Bentley at the University of Maryland. Immobilized metal affinity chromatography columns were purchased from GE Healthcare (Chicago, IL) for protein purification. The glass capillaries were purchased from AIT Glass (Rockaway, NJ). All chemicals were of analytical grade and used without further purification.

Fabrication of a Capillary Microfluidic Device and Drop Generation. We first prepared injection capillaries by tapering circular glass capillaries (1B100-6, World Precision Instruments, Inc., Sarasota, FL) with 560 μm inner diameter to 100 μm inner diameter using a micropipette puller (P-97, Sutter Instrument, Novato, CA). The circular injection capillaries were treated with *n*-octadecyltrimethoxyl silane for 10 min to make the capillary wall hydrophobic and subsequently washed with IPA. The injection capillary was then carefully inserted into a square capillary whose inner width (1.05 mm) is slightly larger than that of the outer diameter of the injection capillary (1 mm). Next, the small tapered glass capillary with a 10 μm inner diameter was prepared by heating and pulling a circular capillary by hand using a gas torch; this capillary was then put into the injection capillary for co-injection of two immiscible fluids. Finally, the circular collection capillary was put into the square capillary from the opposite end; we also treated this collection capillary with *n*-octadecyltrimethoxyl silane to make the capillary wall hydrophobic. To produce triple emulsion drops in a continuous manner, the flow rates of each phase were controlled by syringe pumps (KD Scientific Inc., LEGATO 100, Holliston, MA) and the resulting emulsion drops were observed using an inverted microscope (Eclipse Ti2, Nikon, Japan) equipped with a high-speed camera (Photron USA Inc., MINI UX 50, San Diego, CA).

NHS-Fluorescein Labeling with CS−PEG Core−Shell Microspheres. NHS-fluorescein labeling with as-prepared CS−PEG core−shell microspheres was done as described in our previous work.[35]

Protein Modification with TCO. Protein modification with TCO was carried out as described in our previous work.[24] The final concentrations of the purified TCO-modified R-PE (absorbance peak 565 nm, molar extinction coefficient 1.96×10^6 M^{-1} cm^{-1})[49] and GFPuv (absorbance peak 397 nm, molar extinction coefficient ~ 14,000 M^{-1} cm^{-1})[50] were measured using UV−visible spectroscopy (Evolution 300 UV−vis spectrophotometer, Thermo Scientific).

Protein Conjugation with CS−PEG Core−Shell Microspheres. R-PE and GFPuv conjugation with CS−PEG core−shell microspheres was carried out using Tz-TCO chemistry as described in our previous work.[35]

Production and Purification of GFPuv. Production and purification of GFPuv from *E. coli* BL 21 cells harboring the *ptrcHisB::gfpuv* plasmid were carried out using standard protein expression methods.[51] The as-prepared GFPuv's were quantified via standard Bradford assay[52] and used in the protein conjugation studies without further purification.

Image Analysis. Micrographs of the microspheres were obtained using an epifluorescence microscope (Olympus BX51 equipped with a DP70 microscope digital camera, Centre Valley, PA) and a confocal microscope (Leica DMIRE2 equipped with a TCS SP2 scanner, Wetzlar, Germany), all in SSC−TW20 buffer (pH 7). Epifluorescence micrographs of these microspheres were obtained with a 10× objective lens under standard green (U-N31001), red (U-N31002), and UV (11000v3) filter sets (Chroma Technology Corp., Rockingham, VT). Confocal micrographs were obtained with 10× and 20× objective lens under 488 and 543 nm excitation with depth scan increments of 10−20 μm. Measurements of fluorescence intensity and microsphere diameter were done using ImageJ image analysis software.[53]

ASSOCIATED CONTENT

Supporting Information

The Supporting Information is available free of charge at https://pubs.acs.org/doi/10.1021/acsami.0c20081.

Characterization of core−shell microspheres with SEM and optical microscopy and measurement of interfacial tension and viscosity of the fluids used for the emulsion drops (PDF)

Continuous production of triple emulsion drops in a glass capillary microfluidic device (MP4)

Flow pattern generated in the capillary devices: jetting (MP4)

Flow pattern generated in the capillary devices: non-uniform (MP4)

Flow pattern generated in the capillary devices: separated flow (MP4)

AUTHOR INFORMATION

Corresponding Authors

Hyunmin Yi − *Department of Chemical and Biological Engineering, Tufts University, Medford, Massachusetts 02155, United States;* orcid.org/0000-0002-7750-9679; Email: Hynmin.Yi@tufts.edu

Chang-Hyung Choi − *Division of Cosmetic Science and Technology, Daegu Haany University, Gyeongsan-si, Gyeongsangbuk-do 38610, Republic of Korea;* orcid.org/0000-0002-7561-3720; Email: cchoi@dhu.ac.kr

Authors

Eric Y. Liu − *Department of Chemical and Biological Engineering, Tufts University, Medford, Massachusetts 02155, United States*

https://dx.doi.org/10.1021/acsami.0c20081
ACS Appl. Mater. Interfaces 2021, 13, 11579−11587

Yoon Choi − *Division of Cosmetic Science and Technology, Daegu Haany University, Gyeongsan-si, Gyeongsangbuk-do 38610, Republic of Korea*

Complete contact information is available at: https://pubs.acs.org/10.1021/acsami.0c20081

Author Contributions

E.Y.L. and Y.C. contributed equally. The manuscript was written through contributions of all authors. All authors have given approval to the final version of the manuscript.

Notes

The authors declare no competing financial interest.

■ ACKNOWLEDGMENTS

We gratefully acknowledge partial financial support by the National Research Foundation of Korea (NRF) grant funded by the Korea government (MSIT) (no. 2020R1F1A1056529), the Korea government (MSIT) (no. 2017R1C1B2006237), and the U.S. National Science Foundation (grant # CBET-1703549).

■ REFERENCES

(1) Lee, H.; Kim, J.; Kim, H.; Kim, J.; Kwon, S. Colour-Barcoded Magnetic Microparticles for Multiplexed Bioassays. *Nat. Mater.* **2010**, *9*, 745−749.
(2) Pregibon, D. C.; Toner, M.; Doyle, P. S. Multifunctional Encoded Particles for High-Throughput Biomolecule Analysis. *Science* **2007**, *315*, 1393−1396.
(3) Li, J.; Mooney, D. J. Designing Hydrogels for Controlled Drug Delivery. *Nat. Rev. Mater.* **2016**, *1*, 16071.
(4) Guerzoni, L. P. B.; Bohl, J.; Jans, A.; Rose, J. C.; Koehler, J.; Kuehne, A. J. C.; De Laporte, L. Microfluidic Fabrication of Polyethylene Glycol Microgel Capsules with Tailored Properties for the Delivery of Biomolecules. *Biomater. Sci.* **2017**, *5*, 1549−1557.
(5) Tan, H.; Guo, S.; Dinh, N.-D.; Luo, R.; Jin, L.; Chen, C.-H. Heterogeneous Multi-Compartmental Hydrogel Particles as Synthetic Cells for Incompatible Tandem Reactions. *Nat. Commun.* **2017**, *8*, 663.
(6) Kim, J.; Choi, C.-H.; Yeom, S.-J.; Eom, N.; Kang, K.-K.; Lee, C.-S. Directed Assembly of Janus Cylinders by Controlling the Solvent Polarity. *Langmuir* **2017**, *33*, 7503−7511.
(7) Qi, H.; Ghodousi, M.; Du, Y.; Grun, C.; Bae, H.; Yin, P.; Khademhosseini, A. DNA-Directed Self-Assembly of Shape-Controlled Hydrogels. *Nat. Commun.* **2013**, *4*, 2275.
(8) Le Goff, G. C.; Srinivas, R. L.; Hill, W. A.; Doyle, P. S. Hydrogel Microparticles for Biosensing. *Eur. Polym. J.* **2015**, *72*, 386−412.
(9) Roh, Y. H.; Lee, H. J.; Bong, K. W. Microfluidic Fabrication of Encoded Hydrogel Microparticles for Application in Multiplex Immunoassay. *BioChip J.* **2019**, *13*, 64−81.
(10) Cao, Y.; Zhao, G.; Panhwar, F.; Zhang, X.; Chen, Z.; Cheng, L.; Zang, C.; Liu, F.; Zhao, Y.; He, X. The Unusual Properties of Polytetrafluoroethylene Enable Massive-Volume Vitrification of Stem Cells with Low-Concentration Cryoprotectants. *Adv. Mater. Technol.* **2019**, *4*, 1800289.
(11) Liu, X.; Zhao, G.; Chen, Z.; Panhwar, F.; He, X. Dual Suppression Effect of Magnetic Induction Heating and Microencapsulation on Ice Crystallization Enables Low-Cryoprotectant Vitrification of Stem Cell−Alginate Hydrogel Constructs. *ACS Appl. Mater. Interfaces* **2018**, *10*, 16822−16835.
(12) Zhao, G.; Liu, X.; Zhu, K.; He, X. Hydrogel Encapsulation Facilitates Rapid-Cooling Cryopreservation of Stem Cell-Laden Core−Shell Microcapsules as Cell−Biomaterial Constructs. *Adv. Healthcare Mater.* **2017**, *6*, 1700988.
(13) Chung, B. G.; Lee, K.-H.; Khademhosseini, A.; Lee, S.-H. Microfluidic Fabrication of Microengineered Hydrogels and Their Application in Tissue Engineering. *Lab Chip* **2012**, *12*, 45−59.
(14) Khademhosseini, A.; Langer, R. Microengineered Hydrogels for Tissue Engineering. *Biomaterials* **2007**, *28*, 5087−5092.
(15) Cho, K.; Lee, H. J.; Han, S. W.; Min, J. H.; Park, H.; Koh, W.-G. Multi-Compartmental Hydrogel Microparticles Fabricated by Combination of Sequential Electrospinning and Photopatterning. *Angew. Chem., Int. Ed.* **2015**, *54*, 11511−11515.
(16) Choi, C.-H.; Kang, S.-M.; Jin, S. H.; Yi, H.; Lee, C.-S. Controlled Fabrication of Multicompartmental Polymeric Microparticles by Sequential Micromolding Via Surface-Tension-Induced Droplet Formation. *Langmuir* **2015**, *31*, 1328−1335.
(17) Luo, R.; Cao, Y.; Shi, P.; Chen, C.-H. Near-Infrared Light Responsive Multi-Compartmental Hydrogel Particles Synthesized through Droplets Assembly Induced by Superhydrophobic Surface. *Small* **2014**, *10*, 4886−4894.
(18) Zhang, L.; Chen, K.; Zhang, H.; Pang, B.; Choi, C.-H.; Mao, A. S.; Liao, H.; Utech, S.; Mooney, D. J.; Wang, H.; Weitz, D. A. Microfluidic Templated Multicompartment Microgels for 3d Encapsulation and Pairing of Single Cells. *Small* **2018**, *14*, 1702955.
(19) Peng, B.; van der Wee, E.; Imhof, A.; van Blaaderen, A. Synthesis of Monodisperse, Highly Cross-Linked, Fluorescent Pmma Particles by Dispersion Polymerization. *Langmuir* **2012**, *28*, 6776−6785.
(20) Shi, S.; Zhou, L.; Wang, T.; Bian, L.; Tang, Y.; Kuroda, S.-i. Preparation of Raspberry-Like Poly(Methyl Methacrylate) Particles by Seeded Dispersion Polymerization. *J. Appl. Polym. Sci.* **2011**, *120*, 501−508.
(21) Vivaldo-Lima, E.; Wood, P. E.; Hamielec, A. E.; Penlidis, A. An Updated Review on Suspension Polymerization. *Ind. Eng. Chem. Res.* **1997**, *36*, 939−965.
(22) Plamper, F. A.; Richtering, W. Functional Microgels and Microgel Systems. *Acc. Chem. Res.* **2017**, *50*, 131−140.
(23) Dubbert, J.; Nothdurft, K.; Karg, M.; Richtering, W. Core−Shell−Shell and Hollow Double-Shell Microgels with Advanced Temperature Responsiveness. *Macromol. Rapid Commun.* **2015**, *36*, 159−164.
(24) Gruber, A.; Navarro, L.; Klinger, D. Reactive Precursor Particles as Synthetic Platform for the Generation of Functional Nanoparticles, Nanogels, and Microgels. *Adv. Mater. Interfaces* **2020**, *7*, 1901676.
(25) Dendukuri, D.; Doyle, P. S. The Synthesis and Assembly of Polymeric Microparticles Using Microfluidics. *Adv. Mater.* **2009**, *21*, 4071−4086.
(26) Mitragotri, S.; Lahann, J. Physical Approaches to Biomaterial Design. *Nat. Mater.* **2009**, *8*, 15−23.
(27) Choi, C.-H.; Lee, B.; Kim, J.; Nam, J.-O.; Yi, H.; Lee, C.-S. Controlled Fabrication of Microparticles with Complex 3d Geometries by Tunable Interfacial Deformation of Confined Polymeric Fluids in 2d Micromolds. *ACS Appl. Mater. Interfaces* **2015**, *7*, 11393−11401.
(28) Choi, C.-H.; Lee, H.; Abbaspourrad, A.; Kim, J. H.; Fan, J.; Caggioni, M.; Wesner, C.; Zhu, T.; Weitz, D. A. Triple Emulsion Drops with an Ultrathin Water Layer: High Encapsulation Efficiency and Enhanced Cargo Retention in Microcapsules. *Adv. Mater.* **2016**, *28*, 3340−3344.
(29) Jung, S.; Yi, H. Facile Micromolding-Based Fabrication of Biopolymeric−Synthetic Hydrogel Microspheres with Controlled Structures for Improved Protein Conjugation. *Chem. Mater.* **2015**, *27*, 3988−3998.
(30) Bong, K. W.; Bong, K. T.; Pregibon, D. C.; Doyle, P. S. Hydrodynamic Focusing Lithography. *Angew. Chem., Int. Ed.* **2010**, *49*, 87−90.
(31) Maeda, K.; Onoe, H.; Takinoue, M.; Takeuchi, S. Controlled Synthesis of 3d Multi-Compartmental Particles with Centrifuge-Based Microdroplet Formation from a Multi-Barrelled Capillary. *Adv. Mater.* **2012**, *24*, 1340−1346.
(32) Nie, Z.; Li, W.; Seo, M.; Xu, S.; Kumacheva, E. Janus and Ternary Particles Generated by Microfluidic Synthesis: Design, Synthesis, and Self-Assembly. *J. Am. Chem. Soc.* **2006**, *128*, 9408−9412.

(33) Nisisako, T.; Torii, T.; Takahashi, T.; Takizawa, Y. Synthesis of Monodisperse Bicolored Janus Particles with Electrical Anisotropy Using a Microfluidic Co-Flow System. *Adv. Mater.* **2006**, *18*, 1152−1156.
(34) Seiffert, S. Microgel Capsules Tailored by Droplet-Based Microfluidics. *ChemPhysChem* **2013**, *14*, 295−304.
(35) Liu, E. Y.; Jung, S.; Weitz, D. A.; Yi, H.; Choi, C.-H. High-Throughput Double Emulsion-Based Microfluidic Production of Hydrogel Microspheres with Tunable Chemical Functionalities toward Biomolecular Conjugation. *Lab Chip* **2018**, *18*, 323−334.
(36) Seiffert, S.; Thiele, J.; Abate, A. R.; Weitz, D. A. Smart Microgel Capsules from Macromolecular Precursors. *J. Am. Chem. Soc.* **2010**, *132*, 6606−6609.
(37) Cheng, Y.; Zhang, X.; Cao, Y.; Tian, C.; Li, Y.; Wang, M.; Zhao, Y.; Zhao, G. Centrifugal Microfluidics for Ultra-Rapid Fabrication of Versatile Hydrogel Microcarriers. *Appl. Mater. Today* **2018**, *13*, 116−125.
(38) Choi, C.-H.; Jeong, J.-M.; Kang, S.-M.; Lee, C.-S.; Lee, J. Synthesis of Monodispersed Microspheres from Laplace Pressure Induced Droplets in Micromolds. *Adv. Mater.* **2012**, *24*, 5078−5082.
(39) Lee, H.; Choi, C.-H.; Abbaspourrad, A.; Wesner, C.; Caggioni, M.; Zhu, T.; Nawar, S.; Weitz, D. A. Fluorocarbon Oil Reinforced Triple Emulsion Drops. *Adv. Mater.* **2016**, *28*, 8425−8430.
(40) Arriaga, L. R.; Huang, Y.; Kim, S.-H.; Aragones, J. L.; Ziblat, R.; Koehler, S. A.; Weitz, D. A. Single-Step Assembly of Asymmetric Vesicles. *Lab Chip* **2019**, *19*, 749−756.
(41) Kang, J.-H.; Kim, S.-H.; Fernandez-Nieves, A.; Reichmanis, E. Amplified Photon Upconversion by Photonic Shell of Cholesteric Liquid Crystals. *J. Am. Chem. Soc.* **2017**, *139*, 5708−5711.
(42) Lee, S. S.; Kim, S. K.; Won, J. C.; Kim, Y. H.; Kim, S.-H. Reconfigurable Photonic Capsules Containing Cholesteric Liquid Crystals with Planar Alignment. *Angew. Chem., Int. Ed.* **2015**, *54*, 15266−15270.
(43) Liu, E. Y.; Jung, S.; Yi, H. Improved Protein Conjugation with Uniform, Macroporous Poly(Acrylamide-Co-Acrylic Acid) Hydrogel Microspheres Via Edc/Nhs Chemistry. *Langmuir* **2016**, *32*, 11043−11054.
(44) MacColl, R.; Eisele, L. E.; Williams, E. C.; Bowser, S. S. The Discovery of a Novel R-Phycoerythrin from an Antarctic Red Alga. *J. Biol.* **1996**, *271*, 17157−17160.
(45) Blackman, M. L.; Royzen, M.; Fox, J. M. Tetrazine Ligation: Fast Bioconjugation Based on Inverse-Electron-Demand Diels−Alder Reactivity. *J. Am. Chem. Soc.* **2008**, *130*, 13518−13519.
(46) Vessoni Penna, T. C.; Ishii, M.; Cholewa, O.; De Souza, L. C. Thermal Characteristics of Recombinant Green Fluorescent Protein (Gfpuv) Extracted from Escherichia Coli. *Lett. Appl. Microbiol.* **2004**, *38*, 135−139.
(47) Karver, M. R.; Weissleder, R.; Hilderbrand, S. A. Synthesis and Evaluation of a Series of 1,2,4,5-Tetrazines for Bioorthogonal Conjugation. *Bioconjugate Chem.* **2011**, *22*, 2263−2270.
(48) Sashiwa, H.; Yamamori, N.; Ichinose, Y.; Sunamoto, J.; Aiba, S.-i. Michael Reaction of Chitosan with Various Acryl Reagents in Water. *Biomacromolecules* **2003**, *4*, 1250−1254.
(49) Yu, M.-H.; Glazer, A. N.; Spencer, K. G.; West, J. A. Phycoerythrins of the Red Alga Callithamnion. *Plant Physiol.* **1981**, *68*, 482.
(50) Topell, S.; Hennecke, J.; Glockshuber, R. Circularly Permuted Variants of the Green Fluorescent Protein. *FEBS Lett.* **1999**, *457*, 283−289.
(51) Wu, C.-F.; Cha, H. J.; Rao, G.; Valdes, J. J.; Bentley, W. E. A Green Fluorescent Protein Fusion Strategy for Monitoring the Expression, Cellular Location, and Separation of Biologically Active Organophosphorus Hydrolase. *Appl. Microbiol. Biotechnol.* **2000**, *54*, 78−83.
(52) Bradford, M. M. A Rapid and Sensitive Method for the Quantitation of Microgram Quantities of Protein Utilizing the Principle of Protein-Dye Binding. *Anal. Biochem.* **1976**, *72*, 248−254.
(53) Schneider, C. A.; Rasband, W. S.; Eliceiri, K. W. Nih Image to Imagej: 25 Years of Image Analysis. *Nat. Methods* **2012**, *9*, 671−675.

https://dx.doi.org/10.1021/acsami.0c20081
ACS Appl. Mater. Interfaces 2021, 13, 11579−11587